Journal of Materials Chemistry A

PAPER

View Article Online
View Journal | View Issue

Cite this: J. Mater. Chem. A, 2014, 2, 9306

Flexible and stable lithium ion batteries based on three-dimensional aligned carbon nanotube/silicon hybrid electrodes†

Wei Weng, Huijuan Lin, Xuli Chen, Jing Ren, Zhitao Zhang, Longbin Qiu, Guozhen Guan and Huisheng Peng*

Received 10th February 2014
Accepted 11th March 2014

DOI: 10.1039/c4ta00711e

www.rsc.org/MaterialsA

A three-dimensionally aligned CNT/Si hybrid for flexible and efficient anode has been developed for lithium ion batteries. A delithiation capacity of 2562 mA h g^{-1} was achieved at a current density of 1 A g^{-1} with 93% retention after 100 cycles, and the delithiation capacity was retained at 1055 mA h g^{-1} after 1000 cycles at 5 A g^{-1}. The high specific capacity, cyclic stability and rate performance are ascribed to the aligned CNTs that serve as both conductive pathways and buffer scaffolds to effectively accommodate the volume change of Si in three dimensions. In addition, a stable electrochemical performance is maintained after increasing the areal density of the hybrid anode by over 10 times, indicating great promise for practical applications.

Introduction

Lithium ion batteries (LIBs) have become a leading technology in energy storage for various electronic devices and transport vehicles.[1] Currently, a lot of attention has been paid to developing novel electrode materials and designing new structures aimed at high energy and power densities as well as long life.[2,3] Among the widely studied electrode materials, Si represents one of the most promising candidates due to it having the highest theoretical capacity, *i.e.*, ~4200 mA h g^{-1} for $Li_{4.4}Si$, which is almost eleven times that of commercial graphite.[4] Unfortunately, Si exhibits a dramatic volume change of up to 300% during lithiation/delithiation cycling, leading to pulverization of the Si anode and finally resulting in fast capacity decay.[5,6] A diverse range of approaches have been proposed to overcome this difficulty such as decreasing the dimensions,[7,8] altering the morphology,[9–13] modifying the interfaces[14–16] and designing hybrids.[17–22] It had been demonstrated that the pulverization of Si particles themselves can be mitigated by employing nanoparticles that are smaller than 150 nm.[23] However, electrodes based on bare Si nanoparticles have needed binders and conductive additives and usually failed after only a few dozen cycles due to cracking and disconnection of the electrode. The one-dimensional structures of Si nanowires and nanotubes allowed for a better accommodation of the large volume changes, although improvements were less than expected. Modified interfaces with various voids[14–16] and robust hybrids with framework structures[20,21] have also been designed to accommodate the large volume changes of Si, and high electrochemical performance has been observed. However, as the electrodes produced from the aforementioned approaches involved a lithium-ion slurry manufacturing process, the flexibility of the resulting LIBs was largely limited, even though flexible LIBs are increasingly needed for a wide variety of applications including roll-up displays, wearable electronic devices and implanted medical devices.[24,25] It is important, but it remains challenging to combine high electrochemical performance and flexibility.[26]

To this end, carbon nanotube (CNT)/Si hybrid electrodes[27,28] free of binders and conductive additives and even current collectors that are based on the remarkable mechanical and electrical properties of CNTs[29,30] shed light on the combination of both high capacitance and flexibility. These hybrid electrodes have typically been made into flexible network structures through a simple solution process.[28] However, the electrochemical performance was not as high as expected. Recently, aligned CNTs have also been incorporated as scaffolds for Si in LIBs.[18,31] Similarly, the resulting batteries had limited stability which was insufficient for commercial utility, although good flexibility was realized. Four key characteristics are required for high and stable electrochemical performance in such flexible Si-based hybrid electrodes: (1) a mechanically robust scaffold, (2) continuous electrically conductive pathways, (3) durable bonding between the scaffold and Si and (4) enough space for the volume expansion of Si. Currently available CNT/Si hybrid anodes cannot simultaneously meet these four requirements.

Herein, we have developed a novel three-dimensional (3D) aligned CNT/Si architecture for flexible and efficient anodes. Si is firstly deposited onto an aligned CNT sheet, followed by perpendicular growth of an aligned CNT array on the Si to form a 3D structure. The resulting hybrid films are then cross-stacked into a flexible and free-standing anode without any binders and

State Key Laboratory of Molecular Engineering of Polymers, Department of Macromolecular Science, Laboratory of Advanced Materials, Fudan University, Shanghai 200438, China. E-mail: penghs@fudan.edu.cn

† Electronic supplementary information (ESI) available. See DOI: 10.1039/c4ta00711e

conductive additives. These CNTs aligned in three dimensions serve as a continuous and conductive network as well as a buffer matrix to accommodate the volume change of Si. The Si is sandwiched between aligned CNT sheets and arrays, providing good bonding between the Si and CNTs. Furthermore, the many voids that exist among the aligned CNTs in both the sheets and arrays can effectively accommodate expansion and contraction of the Si. As a result, a delithiation capacity of 2562 mA h g^{-1} was achieved at a current density of 1 A g^{-1} with 93% retention after 100 cycles, and the delithiation capacity remains at 1055 mA h g^{-1} after 1000 cycles at 5 A g^{-1}.

Experimental section

Fig. 1a shows a schematic diagram of the synthesis of the 3D aligned CNT/Si hybrid material. Spinnable carbon nanotube (CNT) arrays were synthesized by chemical vapor deposition.[32] Aligned CNT sheets were dry-drawn from the arrays on a quartz rectangular frame with dimensions of 10 cm × 4 cm. Si was then deposited onto the CNT sheets using electron beam evaporation, and the loading amount of the Si was controlled by varying the deposition time. The catalyst, Fe (1.2 nm)/Al_2O_3 (3 nm), was sequentially deposited onto the Si-coated CNT sheets using electron beam deposition. A perpendicularly aligned CNT array was then grown on the Si-deposited CNT sheet also by chemical vapor deposition. Ethylene was used as a carbon source and a mixture of Ar and H_2 was used as the carrier gas. The flow rates of Ar, H_2, and C_2H_4 were 400, 30 and 90 sccm, respectively. The height of the perpendicular array was controlled by varying the growth time and a height in the range of 2–3 μm, grown in 10 min, was used. The resulting 3D aligned CNT/Si hybrid films could be easily transferred onto various substrates or cross-stacked into the desired LIB hybrid anode. The weights of the components were measured using a microbalance (Sartarious SE2, 0.1 μg resolution). The weight percentage of Si (66%) in the 3D aligned CNT/Si hybrid film was determined using thermogravimetric analysis (Fig. S1†).

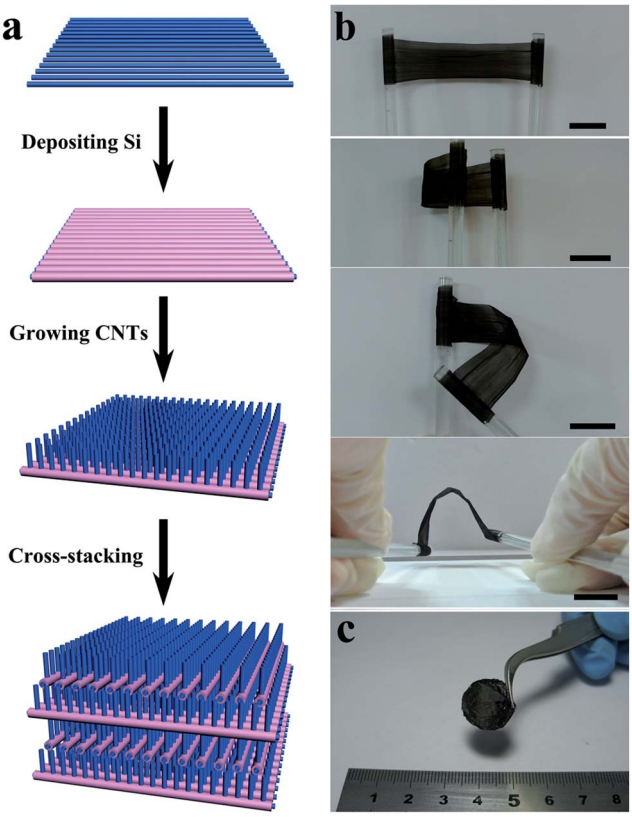

Fig. 1 (a) Schematic illustration of the synthesis of the 3D aligned CNT/Si structure. The blue and pink colors correspond to CNT and Si, respectively. (b) A 3D aligned CNT/Si hybrid material being deformed into various formats. The scale bar corresponds to 2 cm. (c) A 3D aligned CNT/Si hybrid electrode for LIBs.

The structure and morphology were characterized by Raman spectroscopy (Renishaw, inVia), X-ray diffraction (XRD, Bruker, D8 ADVANCE), scanning electron microscopy (SEM, Hitachi, 4800-1) and transmission electron microscopy (TEM, JEOL, JEM-2100F). The LIBs (CR2016 coin type) were assembled in an argon-filled glove-box (Mikrouna, Super 1220/750) with both moisture and oxygen at less than 1 ppm. Electrochemical measurements were conducted using an Arbin BT2000 instrument.

3D aligned CNT/Si hybrid films were directly used as electrodes (without current collectors) with lithium foil as a counter electrode to form an electrochemical half-cell with 1 M $LiPF_6$ in a mixture of ethylene carbonate and diethyl carbonate (volume ratio: 1/1) as the electrolyte. A 3D CNT/Si hybrid film with an areal density of 0.14 mg cm^{-2} was used to investigate the electrochemical performance, except the influence of the areal density on the electrochemical properties. No binders or conductive additives were required for the fabrication of the LIB electrodes. Bare Si film with an areal density of 0.12 mg cm^{-2} on a Cu foil and Si-coated CNT sheets with an areal density of 0.14 mg cm^{-2} were used as control anodes.

Cyclic voltammograms were recorded at a rate of 0.1 mV s^{-1}. Galvanostatic measurements were carried out in a voltage range of 0.005–3 V *versus* Li/Li^+ at different current densities. For the galvanostatic measurements at a current density of 5 A g^{-1}, each electrode was first cycled at a density of 0.5 A g^{-1} for 3 cycles. The specific delithiation capacity of the bare CNTs was initially 267 mA h g^{-1}, when then stabilized at 160 mA h g^{-1} after 100 cycles at a current density of 1 A g^{-1} (Fig. S2†). Therefore, the contribution of the CNTs to the capacity of CNT/Si hybrids was much lower than Si. The applied current densities and the specific capacity were based on the total weight of the electrode, *i.e.*, a weight sum of Si and CNTs. To trace the structural evolution during cycling, the electrodes were soaked in acetonitrile overnight in order to wash off any residual electrolyte and then cleaned by dipping them in an aqueous solution of acetic acid (1 mM) in order to remove the solid electrolyte interface (SEI) layer and other impurities. Finally each electrode was rinsed with deionized water prior to measurement.[33]

Results and discussion

The 3D aligned CNT/Si hybrid anode inherited the good flexibility of the aligned CNT sheet, and could be rolled up and bent into various shapes without breaking (Fig. 1b). For instance, the

tensile strength of the 3D CNT/Si hybrid was traced during cycling, and it was slightly decreased from 65 MPa (with a maximum elongation of 4.1%) prior to cycling to 60 MPa (with a maximum elongation of 3.3%) after cycling (Fig. S3†). Fig. 2a shows a scanning electron microscopy (SEM) image of a CNT sheet that was drawn from the spinnable array. The CNTs are highly aligned along the drawing direction, and they exhibit a multi-walled structure with an average diameter of 12 nm (Fig. S4†). Note that the CNTs appear to have a bundled structure in Fig. 2a after treatment with ethanol during the sample preparation for the SEM observation. Si was uniformly coated onto the CNT sheet and no obvious aggregation was observed (Fig. 2b). In addition, the CNT sheet remained highly aligned after being coated with Si. Interestingly, Si was deposited onto the surfaces of the CNT bundles to form a core–sheath structure (Fig. 2c). The core–sheath hybrid nanotubes exhibited an average diameter of 100 nm. In contrast, it is rare to realize a core–sheath CNT/Si structure based on the previous CNT network.[28] This core–sheath structure can enhance the electrochemical stability as it produces close and stable contact between Si and CNTs as well as a lot of small voids (with sizes of several nanometers) among the aligned CNTs in the CNT bundle and large voids (with sizes of several hundred nanometers) among the Si-deposited CNT bundles that can efficiently withstand any volume change of Si. Fig. 2d and e show top and side views of the 3D aligned CNT/Si hybrid, respectively. The aligned CNT array was perpendicularly grown onto the Si-coated CNT sheet with the height of the array being approximately 3 μm. The CNTs of the sheet underneath retained their original high level of alignment. Interestingly, the aligned CNT array did not peeled off from the Si-coated CNT sheet even after an ultrasonic treatment during preparation of the sample for transmission electron microscopy observations. This phenomenon further verified the stable connection between Si and the CNT arrays for high flexibility and electrochemical performance.

The Si-coated CNT sheet and 3D aligned CNT/Si hybrid were also characterized by Raman spectroscopy and X-ray diffraction (XRD). For the Raman spectra in Fig. 3a, the peak centered at nearly 500 cm^{-1} is related to the Raman phonon vibration of crystalline Si. The crystalline Si peak shifts to lower wavenumbers with decreasing crystallite size.[31] In addition, there are two broad bands at 260–350 cm^{-1} and 890–950 cm^{-1}, which verify the presence of wurtzite Si.[34] Obviously, the growth of the

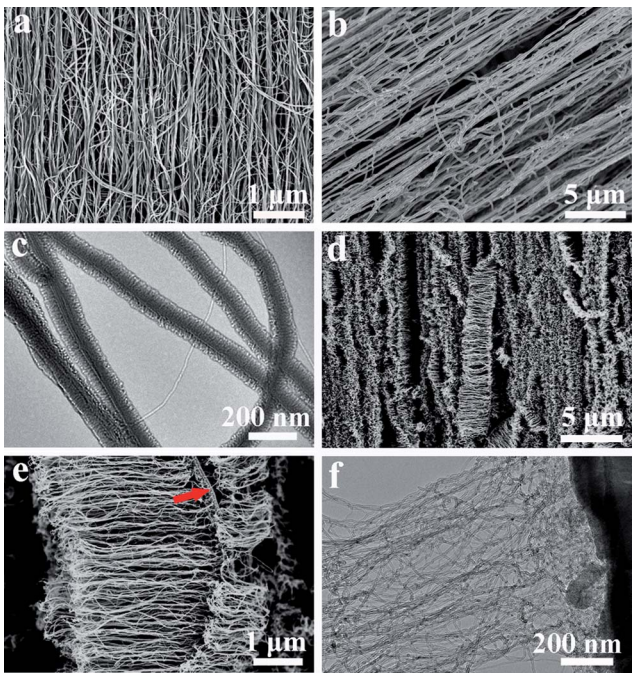

Fig. 2 (a) An SEM image of an aligned CNT sheet. (b) An SEM image of the CNT sheet being deposited with Si. (c) A TEM image of the CNTs coated with Si. (d) and (e) SEM images showing a top and side view of a 3D CNT/Si hybrid, respectively. The red arrow shows the Si-coated CNT sheet. (f) An aligned CNT array on the Si-coated CNT sheet.

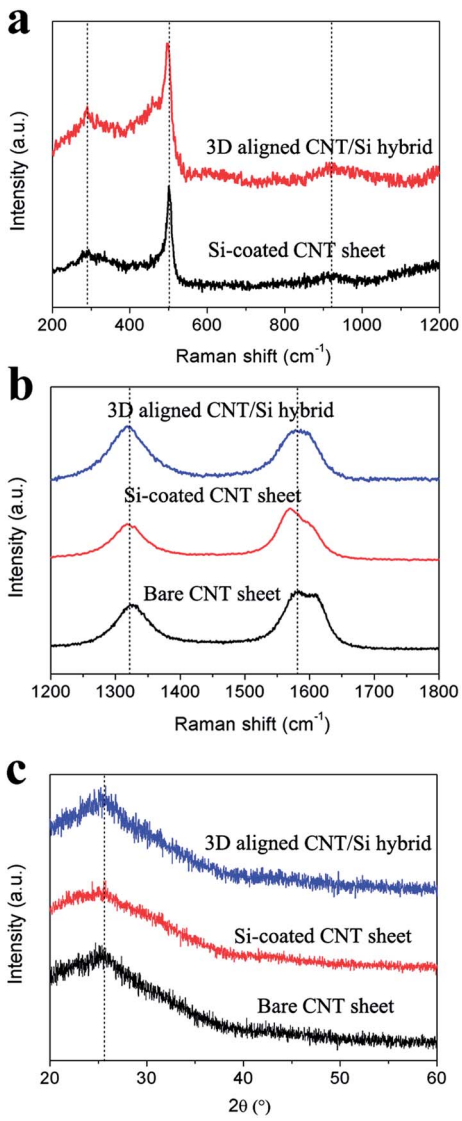

Fig. 3 (a) Raman spectra of the Si component in the Si-coated CNT sheet and 3D aligned CNT/Si hybrid. (b) Raman spectra of the carbon component in the bare CNT sheet, Si-coated CNT sheet and 3D aligned CNT/Si hybrid. (c) X-ray diffraction patterns of the bare CNT sheet, Si-coated CNT sheet and 3D aligned CNT/Si hybrid.

CNT array did not influence the Si morphology. Fig. 3b compares the Raman spectra based on the two characteristic carbon peaks of the D-band (disordered carbon) and G-band (graphitic carbon). The intensity ratio between G and D bands was calculated to be ~1.5 for the CNT sheet, demonstrating the high quality of the CNTs. This ratio remained unchanged after being coated with Si, but was decreased after further growth of the CNT array, indicating the presence of more disordered carbon in the array. At the same time, the G band shifted to a lower wavenumber as expected.[31] Similar to the bare CNT sheet, only the characteristic peak corresponding to the (002) plane of graphite was observed for the CNT/Si hybrid under X-ray diffraction (Fig. 3c), which agreed with a previous report where Si nanoparticles were coated onto CNTs.[31]

Half-cells were assembled to investigate the electrochemical properties of the 3D aligned CNT/Si hybrid with lithium foil as a counter electrode. The charge and discharge corresponded to delithiation and lithiation processes, respectively. Fig. 4a represents typical cyclic voltammetry (CV) spectra. The current peaks at around 1.5 and 0.7 V in the first discharge curve are derived from the formation of SEI layers induced by Si and CNT, respectively.[35,36] The peaks at 0.35 and 0.17 V correspond to the phase transition in amorphous Li_xSi,[37] while the sharp peak at 0.04 V can be attributed to the formation of crystalline $Li_{15}Si_4$.[37,38] The anodic peaks that appear at 0.30 and 0.47 V correspond to the phase transition from amorphous Li_xSi to amorphous Si.[39] The CV spectra were consistent with the charge/discharge curves (Fig. 4b). In contrast to a previous report on pure Si,[11] the 3D CNT/Si hybrid anode delivered a high capacity above 1.0 V (Fig. 4b). This phenomenon may be related to the morphology of the silicon and the interaction between the silicon and the other components in the hybrid. Si films prepared by electron beam evaporation were previously found to deliver a high delithiation capacity above 1.0 V,[40] and silicon-based hybrids have also demonstrated similar behaviour.[18,41] The dependence of the capacity on the cycle number at a current density of 1 A g^{-1} and voltage range of 0.005–3 V *versus* Li/Li^+ is shown in Fig. 4c. The charge capacity reached 2562 mA h g^{-1} at 1 A g^{-1} during the first cycle with a Coulombic efficiency of 71% and 93% of this capacity was maintained after 100 cycles. A

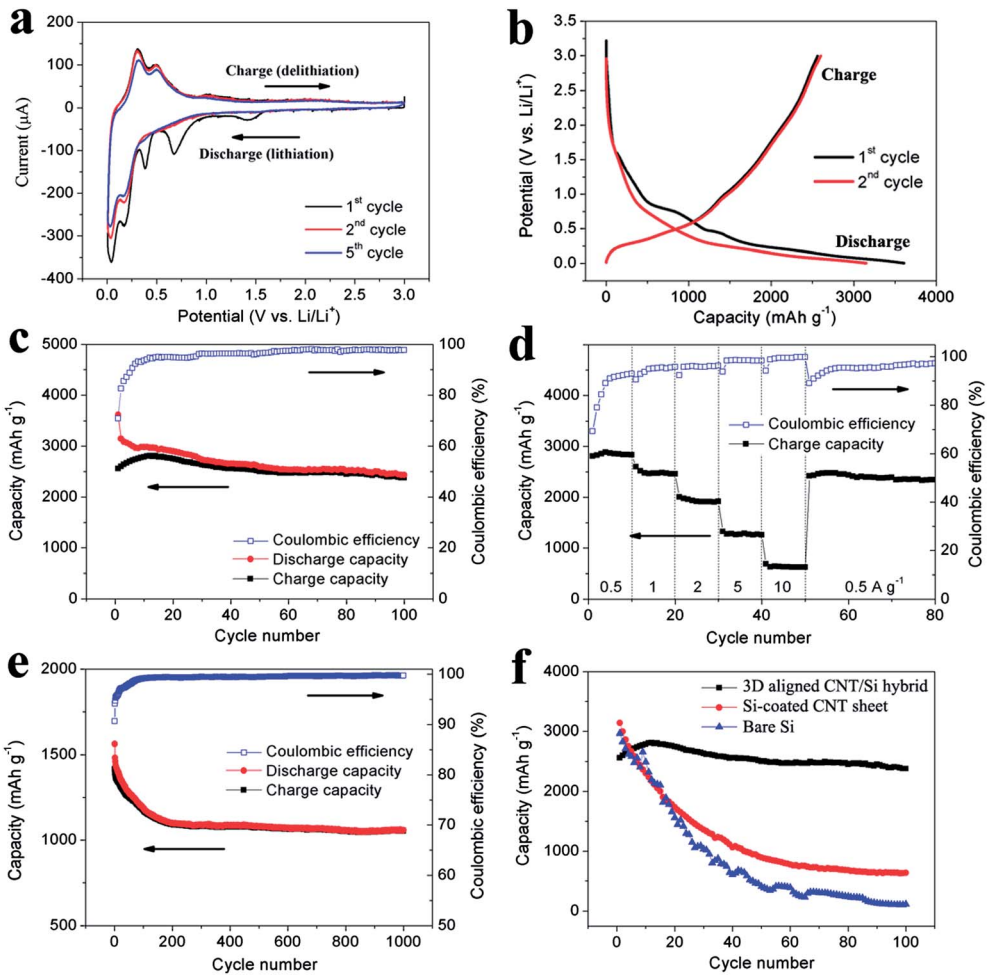

Fig. 4 Electrochemical characterization of the 3D aligned CNT/Si anode between 0.005 and 3 V *versus* Li/Li^+. (a) Cyclic voltammograms at a scan rate of 0.1 mV s^{-1}. (b) Charge/discharge voltage profiles at 0.5 A g^{-1}. (c) Cyclic performance at a current density of 1 A g^{-1}. (d) The cyclic performance at different current densities. (e) Long-life performance over 1000 cycles at 5 A g^{-1}. (f) Comparison of the cyclic performance of the bare CNT sheet, Si-coated CNT sheet and 3D aligned CNT/Si hybrid at 1 A g^{-1}.

slight increase in the capacity occurred in the initial cycles due to the activation of the internal active materials.[42] The theoretical capacity of the 3D CNT/Si hybrid anode was nearly 2450 mA h g^{-1} even though a maximum specific capacity for Si of 3580 mA h g^{-1} in $Li_{15}Si_4$ had been calculated. The measured excess capacity may be related to the solid electrolyte interface, which has been described in other reports.[4,43] The capacity gradually decreased with increasing current density from 0.5 to 10 A g^{-1}, although a charge capacity of nearly 600 mA h g^{-1} was retained even at 10 A g^{-1}, showing a good rate capability (Fig. 4d). To investigate its long-life performance, the anode was cycled 1000 times at a current density of 5 A g^{-1} (Fig. 4e), and a charge capacity of 1055 mA h g^{-1} was achieved with a Coulombic efficiency of 99.7%.

The bare Si films and the Si-coated aligned CNT sheets, *i.e.*, those without the growth of the CNT array, were also compared in Fig. 4f. Both of them exhibited a sharp decrease of the specific capacity with increasing cycle number and the capacity retentions were found to be as low as 4% and 20% after 100 cycles at 1 A g^{-1}, respectively. In contrast, the 3D aligned CNT/Si hybrid achieved 93% capacity retention. Note that a thin Al_2O_3 layer (with a thickness of 3 nm) had to be coated onto the Si as a buffer layer prior to the deposition of an iron film and the growth of the CNT array, and this Al_2O_3 layer also enhances the electrochemical properties by preventing the excessive formation of SEI layers. The huge volume change of Si was found to induce the continuous formation of SEI layers, resulting in the depletion of the electrolyte and degradation of the electrochemical performance.[16] The CV spectra of the Si-coated CNT sheet verified that the SEI formation was decreased by the Al_2O_3 layer (Fig. S5†). However, the hard Al_2O_3 layer underwent cracking upon Si volume expansion.[16] Therefore, the contribution of the Al_2O_3 layer is limited, *e.g.*, the capacity retention of the Si-coated CNT sheet with an Al_2O_3 layer was just 37% after 100 cycles at a rate of 1 A g^{-1} (Fig. S6†).

Additionally, a thin layer of Al_2O_3 film with a thickness of 10 nm was deposited onto the 3D CNT/Si hybrid to further improve the electrochemical performance (Fig. S7†). The Coulombic efficiency was increased by 8% in the first cycle, so this Al_2O_3 coating represents an effective way to decrease the formation of SEI layers. In addition, the stability was also slightly enhanced after 50 cycles at 1 A g^{-1}.

Fig. 5a–c show the structural evolution of the Si-coated CNT sheet after different numbers of cycles. Compared with the original aligned structure, the CNT/Si core–sheath nanotubes became disordered and tangled after 30 cycles at a rate of 1 A g^{-1} (Fig. 5a). The Si layers coated onto the cylindrical substrates were found to swell or shrink only along the radial direction of the generated stress.[44,45] As the stress derived from the volume change of the Si sheath was not uniform, the linear core–sheath CNT/Si hybrid nanotubes may become curved and further tangled with each other. Although the voids among hybrid nanotubes were designed to allow for the expansion of Si, the Si layer peeled off of the CNTs after prolonged cycling (Fig. 5b and c), resulting in poor long-life performance.

In contrast, for the 3D aligned CNT/Si hybrid material, the alignment of the CNT/Si core–sheath nanotubes was well maintained after 30 cycles at a rate of 1 A g^{-1} (Fig. 5d), and the CNT array that was stuck to the Si also retained its highly aligned structure. In addition, the Si layer became thicker and more porous, but did not peel off after 500 cycles at 5 A g^{-1} (Fig. 5e and f). These phenomena indicate that the non-uniform stress generated from the volume change of Si had been effectively buffered by the CNT array. The CNT array favored a stronger bonding between the CNT sheet and Si. Compared with the Si-coated CNT sheet, the 3D aligned CNT/Si hybrid also has more voids due to the porous CNT array. As a result, a high capacity retention of 93% was achieved after 100 cycles at 1 A g^{-1}.

Nanostructured electrodes generally exhibit low areal densities, *e.g.*, 0.1 (ref. 16), 0.17 (ref. 18), 0.2 (ref. 46) and 0.5 (ref. 31) mg cm^{-2} have been shown for Si nanotubes, CNT/Si hybrids, graphene/Si hybrids and Si-coated CNT sheets, respectively, possibly due to low yields and performance degradation with increasing areal density.[47] Therefore, nanostructured electrodes have hardly been used commercially.[47] Recently, it was found that the electrochemical properties can be mostly be retained

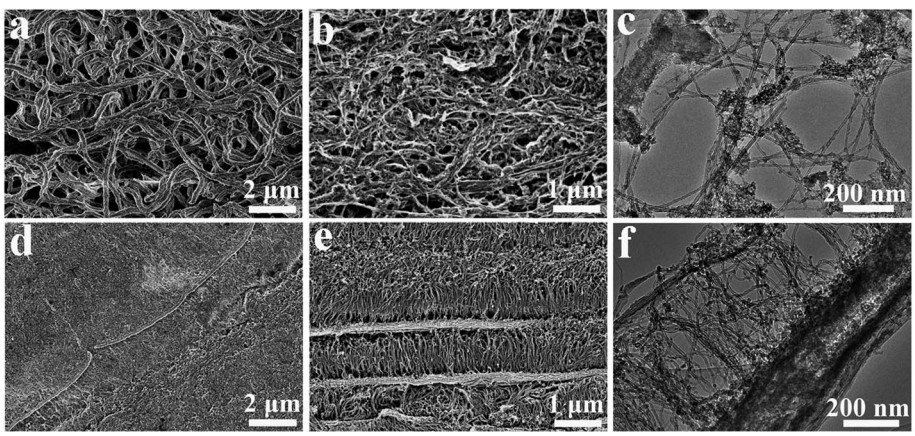

Fig. 5 (a) An SEM image of the Si-coated CNT sheet after 30 cycles at 1 A g^{-1}. (b) and (c) SEM and TEM images of the Si-coated CNT sheet after 500 cycles at 5 A g^{-1}, respectively. (d) An SEM image of the 3D aligned CNT/Si hybrid after 30 cycles at 1 A g^{-1}. (e) and (f) SEM and TEM images of the 3D aligned CNT/Si hybrid after 500 cycles at 5 A g^{-1}. The voltage was varied between 0.005 and 3 V *versus* Li/Li^+.

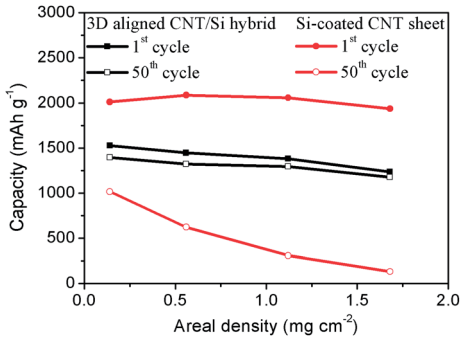

Fig. 6 Impact of the areal density on the specific capacity at 5 A g^{-1}.

when increasing the areal density from 0.175 to 0.7 mg cm^{-2} using vertical CNT arrays as a skeleton in a hybrid anode.[48] In the proposed aligned CNT/Si hybrid, the 3D network made of aligned CNTs can achieve these merits in a much better fashion. Fig. 6 compares the dependence of the electrochemical performance on the areal density for the Si-coated CNT sheets and the 3D aligned CNT/Si hybrid. The areal density was easily increased by cross-stacking more layers for both materials, *e.g.*, increasing from 0.14 to 1.68 mg cm^{-2}. However, for the Si-coated CNT sheets, a fast decrease in capacity occurred in the 50th cycle with increasing areal density. In contrast, a stable capacity was maintained in the 3D aligned CNT/Si hybrid, which meets the commercial requirements for LIBs.

Conclusion

In summary, a novel 3D aligned CNT/Si hybrid material has been developed as free-standing, flexible and efficient anode in LIBs. The designed CNTs aligned in three dimensions, simultaneously serve as a strong scaffold and provide conductive pathways to better accommodate the volume change of Si and enable high and stable electrochemical performance. For instance, a delithiation capacity of 2562 mA h g^{-1} was achieved at a current density of 1 A g^{-1} with 93% retention after 100 cycles. This work also presents a general and effective strategy for developing promising electrode materials for high performance electronic devices.

Acknowledgements

This work was supported by NSFC (91027025, 21225417), MOST (2011CB932503, 2011DFA51330), STCSM (11520701400, 12nm0503200), the Fok Ying Tong Education Foundation, The Program for Professor of Special Appointment at Shanghai Institutions of Higher Learning, and the Program for Outstanding Young Scholars from the Organization Department of the CPC Central Committee.

References

1 B. Dunn, H. Kamath and J. M. Tarascon, *Science*, 2011, **334**, 928.
2 J. Liu and X. W. Liu, *Adv. Mater.*, 2012, **24**, 4097.
3 M. G. Kim and J. Cho, *Adv. Funct. Mater.*, 2009, **19**, 1497.
4 J. R. Szczech and S. Jin, *Energy Environ. Sci.*, 2011, **4**, 56.
5 U. Kasavajjula, C. Wang and A. J. Appleby, *J. Power Sources*, 2007, **163**, 1003.
6 H. Wu and Y. Cui, *Nano Today*, 2012, **7**, 414.
7 H. Kim, M. Seo, M. H. Park and J. Cho, *Angew. Chem., Int. Ed.*, 2010, **49**, 2146.
8 A. Magasinski, P. Dixon, B. Hertzberg, A. Kvit, J. Ayala and G. Yushin, *Nat. Mater.*, 2010, **9**, 353.
9 H. Ma, F. Cheng, J. Y. Chen, J. Z. Zhao, C. S. Li, Z. L. Tao and J. Liang, *Adv. Mater.*, 2007, **19**, 4067.
10 Y. He, X. Yu, Y. Wang, H. Li and X. Huang, *Adv. Mater.*, 2011, **23**, 4938.
11 C. K. Chan, H. Peng, G. Liu, K. McIlwrath, X. F. Zhang, R. A. Huggins and Y. Cui, *Nat. Nanotechnol.*, 2008, **3**, 31.
12 M. H. Park, G. K. Kim, J. Joo, K. Kim, J. Kim, S. Ahn, Y. Cui and J. Cho, *Nano Lett.*, 2009, **9**, 3844.
13 M. R. Zamfir, H. T. Nguyen, E. Moyen, Y. H. Lee and D. Pribat, *J. Mater. Chem. A*, 2013, **1**, 9566.
14 N. Liu, H. Wu, M. T. McDowell, Y. Yao, C. Wang and Y. Cui, *Nano Lett.*, 2012, **12**, 3315.
15 T. H. Hwang, Y. M. Lee, B. S. Kong, J. S. Seo and J. W. Choi, *Nano Lett.*, 2012, **12**, 802.
16 H. Wu, G. Chan, J. W. Choi, I. Ryu, Y. Yao, M. T. McDowell, S. W. Lee, A. Jackson, Y. Yang, L. Hu and Y. Cui, *Nat. Nanotechnol.*, 2012, **7**, 309.
17 R. Yi, F. Dai, M. L. Gordin, S. Chen and D. Wang, *Adv. Energy Mater.*, 2013, **3**, 295.
18 A. Gohier, B. Laik, K. H. Kim, J. L. Maurice, J. P. Pereira-Ramos, C. S. Cojocaru and P. Van Tran, *Adv. Mater.*, 2012, **24**, 2592.
19 D. P. Wong, H. P. Tseng, Y. T. Chen, B. J. Hwang, L. C. Chen and K. H. Chen, *Carbon*, 2013, **63**, 397.
20 G. Liu, S. Xun, N. Vukmirovic, X. Song, P. Olalde-Velasco, H. Zheng, V. S. Battaglia, L. Wang and W. Yang, *Adv. Mater.*, 2011, **23**, 4679.
21 H. Wu, G. Yu, L. Pan, N. Liu, M. T. McDowell, Z. Bao and Y. Cui, *Nat. Commun.*, 2013, **4**, 1943.
22 S. A. Klankowski, R. A. Rojeski, B. A. Cruden, J. Liu, J. Wu and J. Li, *J. Mater. Chem. A*, 2013, **1**, 1055.
23 X. H. Liu, L. Zhong, S. Huang, S. X. Mao, T. Zhu and J. Y. Huang, *ACS Nano*, 2012, **6**, 1522.
24 S. Xu, Y. Zhang, J. Cho, J. Lee, X. Huang, L. Jia, J. A. Fan, Y. Su, J. Su, H. Zhang, H. Cheng, B. Lu, C. Yu, C. Chuang, T. I. Kim, T. Song, K. Shigeta, S. Kang, C. Dagdeviren, I. Petrov, P. V. Braun, Y. Huang, U. Paik and J. A. Rogers, *Nat. Commun.*, 2013, **4**, 1543.
25 Y. H. Kwon, S. W. Woo, H. R. Jung, H. K. Yu, K. Kim, B. H. Oh, S. Ahn, S. Y. Lee, S. W. Song, J. Cho, H. C. Shin and J. Y. Kim, *Adv. Mater.*, 2012, **24**, 5192.
26 S. Park, M. Vosguerichian and Z. Bao, *Nanoscale*, 2013, **5**, 1727.
27 K. Evanoff, J. Benson, M. Schauer, I. Kovalenko, D. Lashmore, W. J. Ready and G. Yushin, *ACS Nano*, 2012, **6**, 9837.

28 L. F. Cui, L. B. Hu, J. W. Choi and Y. Cui, *ACS Nano*, 2010, **4**, 3671.
29 M. F. Yu, B. S. Files, S. Arepalli and R. S. Ruoff, *Phys. Rev. Lett.*, 2000, **84**, 5552.
30 V. Meunier, J. Kephart, C. Roland and J. Bernholc, *Phys. Rev. Lett.*, 2002, **88**, 075506.
31 K. Fu, O. Yildiz, H. Bhanushali, Y. Wang, K. Stano, L. Xue, X. Zhang and P. D. Bradford, *Adv. Mater.*, 2013, **25**, 5109.
32 S. Huang, L. Li, Z. Yang, L. Zhang, H. Saiyin, T. Chen and H. Peng, *Adv. Mater.*, 2011, **23**, 4707.
33 J. W. Choi, J. McDonough, S. Jeong, J. S. Yoo, C. K. Chan and Y. Cui, *Nano Lett.*, 2010, **10**, 1409.
34 M. A. Mohiddon and M. G. Krishna, *J. Phys. Chem. Solids*, 2013, **74**, 1249.
35 S. Y. Chew, S. H. Ng, J. Wang, P. Novák, F. Krumeich, S. L. Chou, J. Chen and H. K. Liu, *Carbon*, 2009, **47**, 2976.
36 J. Eom, D. Kim and H. Kwon, *J. Power Sources*, 2006, **157**, 507.
37 C. Y. Du, C. H. Gao, G. P. Yin, M. Chen and L. Wang, *Energy Environ. Sci.*, 2011, **4**, 1037.
38 H. T. Nguyen, M. R. Zamfir, L. D. Duong, Y. H. Lee, P. Bondavalli and D. Pribat, *J. Mater. Chem.*, 2012, **22**, 24618.
39 M. N. Obrovac and L. J. Krause, *J. Electrochem.Soc.*, 2007, **154**, A103.
40 S. Ohara, J. Suzuki, K. Sekine and T. Takamura, *J. Power Sources*, 2004, **136**, 303.
41 L. W. Ji and X. W. Zhang, *Energy Environ. Sci.*, 2010, **3**, 124.
42 J. Deng, H. Ji, C. Yan, J. Zhang, W. Si, S. Baunack, S. Oswald, Y. Mei and O. G. Schmidt, *Angew. Chem., Int. Ed.*, 2013, **52**, 2326.
43 C. K. Chan, R. N. Ratel, M. J. O'Connell, B. A. Korgel and Y. Cui, *ACS Nano*, 2010, **4**, 1443.
44 C. M. Wang, X. Li, Z. Wang, W. Xu, J. Liu, F. Gao, L. Kovarik, J. G. Zhang, J. Howe, D. J. Burton, Z. Liu, X. Xiao, S. Thevuthasan and D. R. Baer, *Nano Lett.*, 2012, **12**, 1624.
45 M. Gu, Y. Li, X. L. Li, S. Y. Hu, X. W. Zhang, W. Xu, S. Thevuthasan, D. R. Baer, J. G. Zhang, J. Liu and C. Wang, *ACS Nano*, 2012, **6**, 8439.
46 C. Wang, Y.-S. Chui, R. Ma, T. Wong, J.-G. Ren, Q.-H. Wu, X. Chen and W. Zhang, *J. Mater. Chem. A*, 2013, **1**, 10092.
47 Y. Gogotsi and P. Simon, *Science*, 2011, **334**, 917.
48 Q. Xiao, Y. Fan, X. Wang, R. A. Susantyoko and Q. Zhang, *Energy Environ. Sci.*, 2014, **7**, 655.